Semiconductor Physics, Quantum Electronics & Optoelectronics, 2021. V. 24, No 4. P. 390-398.

Semiconductor physics

Peculiarities of specular infrared reflection spectra of ZnO-based ceramics

O.V. Melnichuk[1,*], N.O. Korsunska[2], I.V. Markevich[2], V.V. Boyko[3], Yu.O. Polishchuk[2], Z.F. Tsybrii[2], L.Yu. Melnichuk[1], Ye.F. Venger[2], V.P. Kladko[2], L.Yu. Khomenkova[2,4,]**

[1]*Mykola Gogol State University of Nizhyn, 2, Hrafska str., 16600 Nizhyn, Ukraine*
[2]*V. Lashkaryov Institute of Semiconductor Physics, NAS of Ukraine, 45, prosp. Nauky, 03680 Kyiv, Ukraine*
[3]*Institute of Physics, NAS of Ukraine, 46, prosp. Nauky, 03680 Kyiv, Ukraine*
[4]*National university "Kyiv Mohyla Academy", 2, Skovorody str., 04070 Kyiv, Ukraine*
E-mail: mov310310@gmail.com[*]; khomen@ukr.net[**]

Abstract. Undoped and Mn-doped ZnO ceramics were theoretically and experimentally investigated using specular infrared reflection method. It was shown that infrared reflection spectra can be modeled using the parameters explored for ZnO single crystals. For ceramic samples, it was shown that ZnO grains with orientation of the *C*-axis along the normal to the electric field ($\vec{E} \perp C$) give the main contribution to IR reflection spectra. It has been ascertained that the surface roughness is manifested in these spectra mainly within the range 450…550 cm^{-1} giving negligible effect for the frequencies above longitudinal phonon frequency. This allowed the electrophysical parameters of ZnO crystallites to be evaluated. In the case of undoped ceramics, the obtained results were found to be consistent with the values of direct current measurements. This finding supports the utility of infrared spectroscopy for determination of the electrophysical parameters of polycrystalline ceramic materials. For Mn-doped ceramic samples, the conductivity value measured using the direct current method was found to be essentially lower than those determined from simulation of infrared reflection spectra. This phenomenon was explained by barrier formation at the grain boundaries in Mn-doped ZnO ceramics.

Keywords: ZnO, ceramics, infrared spectroscopy, doping, conductivity.

https://doi.org/10.15407/spqeo24.04.390
PACS 78.20.Bh, 78.30.-j, 81.20.-n, 81.70.-q

Manuscript received 27.08.21; revised version received 04.10.21; accepted for publication 10.11.21; published online 23.11.21.

1. Introduction

Materials based on zinc oxide (ZnO) attract significant attention due to unique physicochemical properties, which allow wide applications. However, production of perfect single crystals requires specific equipment operating at high-temperature and high-pressure regimes [1, 2]. Due to complexity of single crystal growth, the interest of researchers to ZnO-based ceramics and thin films increased in recent decades. These ZnO-based materials found their application as transparent conductive electrodes [3, 4], in microelectronics [5], for light-emitting devices [6, 7], in varistors [8, 9], for photocatalysis [10, 11], *etc*.

It is worth to point out that, contrary to the ZnO single crystals [1, 12], the investigation of electrophysical properties of ZnO films and ceramics is usually faced with some difficulties due to their polycrystalline nature [7, 13].

Infrared reflection (IRR) spectroscopy is one of the non-destructive methods allowed establishing electrophysical parameters [14, 15]. However, this method was not often addressed. At the same time, it allows the conductivity, free carrier concentration and mobility of undoped and doped ZnO single crystals to be determined [12–15]. In particular, it was found that ZnO is characterized by strong anisotropy of phonon properties and slight anisotropy of the plasmon subsystem [12, 14]. In [15, 16], the specular reflection spectra from the ZnO crystals with an electron concentration varied from 10^{16} to $5\cdot10^{19}$ cm^{-3} were experimentally investigated and self-consisted parameters for those single crystals were obtained. In [17], for the first time, the oscillations of three pair-linked subsystems were taken into account, namely: electromagnetic waves, optical lattice oscillations and free carriers plasma oscillations for perpendicular and parallel orientations of electric field vector $\vec{E}$ to the *C*-axis ($\vec{E} \perp C$ and $\vec{E} \parallel C$ orientations, respectively).

Recently, we have demonstrated that the IRR method can be applied for studying the optical and electrophysical properties of undoped and doped ZnO thin films grown on both dielectric and semiconductor substrates by means of magnetron sputtering [18, 19] and atomic layer deposition [20]. It was shown that in these films, the *C*-axis of ZnO crystallites was mainly oriented along the normal to the film/substrate interface. This allowed theoretical modeling of IRR spectra within the range 50…1500 cm^{-1} for the $\vec{E} \perp C$ orientation to be performed. The optical and electrical parameters of ZnO-based films, as well as the oscillator strengths and the values of their damping coefficients for the films and the substrates were determined using a multi-oscillator model. In this case, the influence of phonon and plasmon-phonon subsystems of the substrates on the shape of the IRR spectra of ZnO film/dielectric (semiconductor) substrate structure was taken into account.

Despite significant interest to ZnO-based materials, application of the IRR method for the characterization of ZnO ceramics was not well addressed. At the same time, this method is able to provide important information on polycrystalline samples, for instance, textured films and ceramics. Indeed, for these samples there is a difficulty to determine the free carrier concentration (n_0) and mobility (μ) by using the conventional methods (measurement of direct current conductivity or the Hall effect study). The main reason is the presence of barriers at the grain boundaries, as it was reported for ZnO films obtained using magnetron sputtering [19, 21] and for ZnO ceramics doped with various impurities [22 and references therein]. In this case, information on the n_0 and μ values was extracted from the IRR spectra.

It is worth to note that in comparison to single crystals and textured films, ceramics have significant differences. Firstly, it is the presence of crystallites with different optical axis orientations in relation to the direction of light incidence, and secondly, a certain surface roughness, which can complicate obtaining information about the electrical parameters of the crystallites. Indeed, the light wave reflected by the surface of the ZnO single crystal is formed in the near-surface layer [12, 14, 15]. Optically polished ZnO crystals have higher surface roughness than those with cleavage surface and, consequently, the magnitude of corresponding IRR signal in the "residual rays" range ("reststrahlen band") decreases regardless to the optical axis orientation [23]. Similar results were reported for CdTe crystals in Ref. [24]. Therefore, the study of the influence of the above mentioned factors on the IRR spectra is required to determine the ceramic characteristics.

The aim of this work is to elucidate the peculiarities of specular IRR spectra of ZnO ceramic samples as well as the possibility of applying this contactless method for determination the optical and electrophysical parameters of ZnO crystallites in ceramic materials.

2. Experimental details and methods

Undoped and manganese-doped ZnO ceramics were prepared from a mixture of ZnO powder (99.99% purity) with distilled water or aqueous $MnSO_4$ solution, respectively. After drying at room temperature for 24 hours, the mixtures were pressed into the pellets with the dimensions in the length, width and thickness of 20×8×3 mm. The used pressure was 20 MPa. These pellets were subsequently annealed in muffle furnace at 1000 °C for 3 hours in air being naturally cooled with the furnace to room temperature. The pellets were cleft transversally in several parts with average sizes of 2×5×1 mm. They were additionally polished to reduce the roughness of the ceramic surface. The concentration of manganese in the doped samples was about 10^{20} cm^{-3}.

ZnO single crystals with different free carrier concentrations were also studied. These crystals were grown using the hydrothermal method [14, 15] and then were cut as parallelepipeds with the dimensions of 10×8×8 mm. All their sides were optically polished. In this work, ZnO single crystals were used as a model object allowed to determine the effect of the *C*-axis orientation and the n_0 value on the IRR spectra. Experimental IRR spectra (called hereafter as $R_E(\nu)$) were measured for $\vec{E} \perp C$ and $\vec{E} \| C$ orientations, and these results were further used for the analysis of the IRR spectra of ceramic samples.

Specular IRR spectra of the ceramics were measured using a Bruker Vertex 70 V FTIR spectrometer at the angle of excitation light incidence 13°. A gold mirror was used as a reference. The spectra were recorded with a resolution of 1 cm^{-1}. The error of reflection coefficient measurements was about 1%. More details can be found in [19, 22]. The structure of samples was investigated by means of the X-ray diffraction (XRD) method. XRD patterns were recorded in Bragg-Brentano geometry using a Philips X'Pert-MRD diffractometer with $CuK_{\alpha 1}$ radiation. In addition, measurements of the direct current (DC) conductivity were performed. To do this, indium Ohmic contacts were deposited on cleavage surfaces of opposite sides.

3. Results and discussion

3.1. Structural properties of ceramic samples (XRD data)

Fig. 1 shows the XRD patterns of undoped and Mn-doped ZnO ceramics. All XRD peaks correspond to hexagonal ZnO and the ratio of their intensities does not show any predominant orientation of ZnO crystallites (according to the ICDD card #010-70-8072), which indicates a random orientation of crystallite *C*-axis. The XRD pattern of Mn-doped ZnO sample is similar to that of undoped one. Any other phases including Mn-related ones were not detected in all the samples.

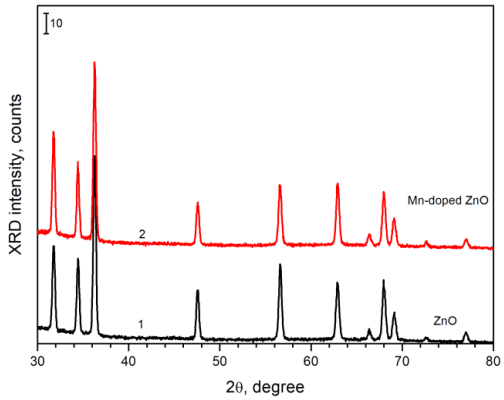

Fig. 1. XRD patterns of undoped (*1*) and Mn-doped (*2*) ZnO ceramics.

3.2. Specular IRR spectra

3.2.1. IRR spectra of ZnO single crystals

The group theory predicts the existence of nine optical and three acoustic branches in ZnO [15]. Two optical modes (E_1 and A_1) are doubly degenerated and active in the IR spectral range.

Since a mixed ion-covalent bond is formed between atoms in ZnO, the long-range Coulomb field leads to the splitting of E_1- and A_1-type oscillations into longitudinal and transverse components. The corresponding frequencies of transverse optical oscillations E_1 and A_1 were called as $\nu_{T_\perp}$ and $\nu_{T_\parallel}$ and longitudinal one A_1 – as $\nu_{L_\perp}$ and $\nu_{L_\parallel}$. The symbols $\parallel$ and $\perp$ mean the polarization of the phonon parallel and perpendicular to the *C*-axis, respectively. It should be noted that the modes associated with the combination of phonons can be also observed. In particular, this can be the result of doping [25].

Table 1 shows ZnO crystal structure and the types of phonons for different polarizations and directions of propagation. As one can see, there are three possible modes of oscillations in the *Z*-direction: $T_\perp$ mode polarized in the *X*-direction, similar $T_\perp$ mode polarized in the *Y*-direction and $L_\parallel$ mode polarized in the *Z*-direction.

Table 1. Schematic illustration of ZnO crystal structure and types of phonons for different polarizations and propagation directions.

Direc-tion of phonon propa-gation	Phonon polarization		
	$X(E_1)$	$Y(E_1)$	$Z(A_1)$
Ox	$L_\perp$	$T_\perp$	$T_\parallel$
Oy	$T_\perp$	$L_\perp$	$T_\parallel$
Oz	$T_\perp$	$T_\perp$	$L_\parallel$

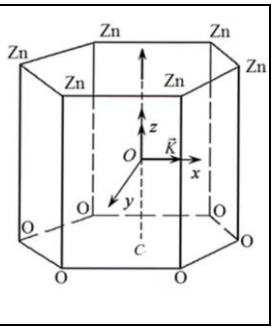

Table 2. Optical parameters of ZnO single crystal.

ZnO	ε_0	ε_∞	ν_T, cm^{-1}	ν_L, cm^{-1}
$E \perp C$	8.1	3.95	412	591
$E \parallel C$	9.0	4.05	380	570

If phonon propagates along the *X*- and *Y*-axes (*Z*-axis coincides with the direction of the optical *C*-axis), then only pure LO phonons are observed, which corresponds to the IRR spectra measured for the case $\vec{E} \perp C$ (Fig. 2, triangle symbols (▲)). When phonon propagates along the *Z*-axis, only TO phonons appear in the IRR spectrum corresponding to the case $\vec{E} \parallel C$ (Fig. 2, dot symbols (●)). As follows from Table 1, only in the case of A_1-mode excitation in the *Z*-direction that coincides with the direction of the *C*-axis, it is possible to observe the IRR spectrum for $\vec{E} \parallel C$. In all other cases, the IRR spectrum with $\vec{E} \perp C$ orientation will be registered.

Dispersion analysis of the IRR spectra of ZnO crystals in the "residual rays" range allowed obtaining the optical parameters of ZnO single crystal (Table 2). These parameters were found to be similar to those reported earlier [14, 16] and they were further used for fitting the IRR spectra of ZnO-based ceramic samples.

Theoretical IRR spectra (called hereafter as $R_T(\nu)$) were also simulated as based on the approach described in [14, 18, 20–22]. Frequency dependence of dielectric constant $\varepsilon(\nu)$ within the spectral range corresponding to the plasmon-phonon interaction was presented using the Helmholtz–Kettler formula:

$$\varepsilon(\nu) = \varepsilon_1 + i\varepsilon_2 = \varepsilon_\infty + \varepsilon_f + \varepsilon_p, \qquad (1)$$

where ε_∞ is high-frequency dielectric constant, ε_f is the contribution of active optical phonons with the frequencies ν_T and ν_L, ε_p – contribution of free carriers (the plasmon frequency is denoted as ν_p).

If the values of ν_T, ν_L and ν_p as well as corresponding damping coefficients of phonons (γ_f) and plasmons (γ_p) are known, then Eq. (1) can be considered *versus* IR light frequency ν as

$$\varepsilon(\nu) = \varepsilon_\infty + \frac{\varepsilon_\infty\left(\nu_L^2 - \nu_T^2\right)}{\nu_T^2 - \nu^2 + i\nu\gamma_f} - \frac{\varepsilon_\infty \nu_p^2}{\nu\left(\nu + i\nu\gamma_p\right)}. \qquad (2)$$

Being based on the interrelation of dielectric constant $\varepsilon(\nu)$ with the refractive index ($n(\nu)$) and extinction coefficient ($k(\nu)$) [14], the reflection coefficient can be found as

$$R(\nu) = \frac{(n(\nu)-1)^2 + k(\nu)^2}{(n(\nu)+1)^2 + k(\nu)^2}, \qquad (3)$$

taking into account the contribution of bulk phonons and plasmons. The results obtained for $E \perp C$ and $E \parallel C$ are shown in Fig. 2 by the curves *1* and *2*, respectively.

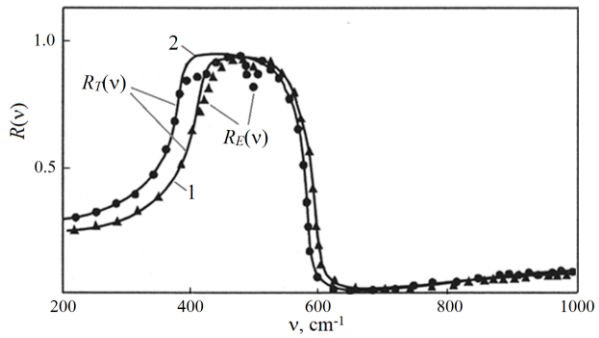

Fig. 2. IRR spectra of ZnO single crystal ($R_E(\nu)$) for $\vec{E} \perp C$ (▲) and $\vec{E} \| C$ (●) and corresponding fitting ($R_T(\nu)$) with the parameters: *1* – ν_P = 90 cm^{-1}, γ_P = 150 cm^{-1}, γ_f = 11 cm^{-1}, $\delta = 0.29 \cdot 10^{-2}$; *2* – ν_P = 100 cm^{-1}, γ_P = 170 cm^{-1}, γ_f = 11 cm^{-1}, $\delta = 0.29 \cdot 10^{-2}$.

This simulation was performed for the 200…1000-cm^{-1} spectral range varying the value of damping coefficient for TO phonon (γ_f). It turned out that the best fitting corresponds to the modeling with γ_f = 11 cm^{-1}. The standard deviation δ was $0.29 \cdot 10^{-2}$ (~ 0.3%).

As one can see from Fig. 2, there is a difference between $R_E(\nu)$ and $R_T(\nu)$ within the range 400…480 cm^{-1}. This difference is caused by the surface roughness and surface defects. Apart from this, the $R_E(\nu)$ data show a minimum at ν = 504 cm^{-1} that can be a result of the presence of lithium impurities observed usually in hydrothermally grown ZnO crystals [14]. Besides, this minimum can be a sign of surface optical phonon vibrations occurred in disordered surface of ZnO crystal or grain boundaries [1, 5].

Fig. 2 demonstrates anisotropy of the optical properties of ZnO in the "residual rays" range. The spectrum for $E \| C$ is shifted towards the lower frequencies as compared to the spectrum for $E \perp C$, and the largest difference in the spectra is observed in the range of TO phonon (200…400 cm^{-1}). At the same time, the values of the reflection coefficients at the reflection maxima coincide.

In ceramic samples, ZnO crystallites with different orientation of their optical axis are present. Taking this fact into account, a theoretical calculation of the IRR spectra for different orientation of *C*-axis from $E \| C$ to $E \perp C$ and $\gamma_{f\perp}$ = 11 cm^{-1} was performed (Fig. 3). The angles between the *C*-axis and the vector *E* were chosen to be φ = 90° (curve *1*), 60° (curve *2*), 45° (curve *3*), 30° (curve *4*), 0° (curve *5*).

As it can be seen from Fig. 3, the significant changes in the IRR spectra are observed for φ = 30, 45, and 60°, and they are manifested in the appearance of a minimum reflection coefficient within the range of LO phonon (570…590 cm^{-1}), which allows us to offer the optical method for determining the orientation of optical axis in ZnO materials. Simultaneously, a gradual shift of the $R_T(\nu)$ curve towards the lower frequencies in the range of TO phonon is observed, when the orientation changes from $E \perp C$ to $E \| C$.

To determine the effect of the free carrier concentration on the IRR spectra, their theoretical calculation was performed at different $\nu_{p\perp}$ and $\gamma_{p\perp}$ values (Fig. 4). The spectra were calculated for the orientation $E \perp C$ at $\gamma_{f\perp}$ = 11 cm^{-1}, whereas $\nu_{p\perp}$ and $\gamma_{p\perp}$ were taken to be equally changed from 1 to 1000 cm^{-1} (curves *1* to *5*). It is seen that the most significant changes in the IRR spectra are observed at $\nu_{p\perp} = \gamma_{p\perp}$ = 500…1000 cm^{-1}, which corresponds to the concentrations $n_0 = 10^{18}…10^{20}$ cm^{-3}.

Thus, as can be seen from Figs 2 to 4, the analysis of IRR spectra allows obtaining information on the optical and electrophysical parameters of ZnO, in particular, the conductivity, concentration and mobility of free carriers can be estimated along with the orientation of the optical axis of crystals and their surface quality.

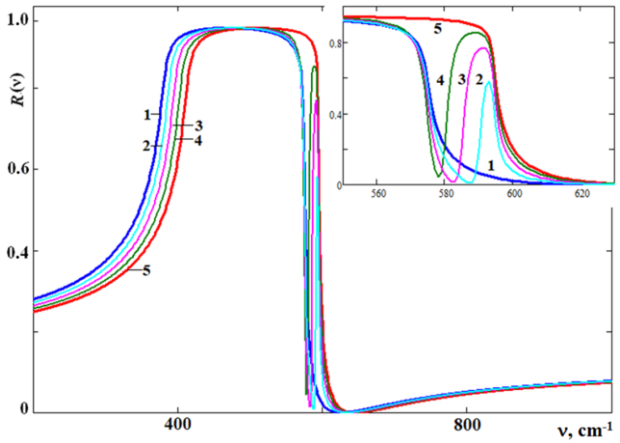

Fig. 3. Simulated $R_T(\nu)$ spectra of ZnO single crystal for different orientation of *C*-axis, from $E \| C$ (*1*) to $E \perp C$ (*5*) – φ = 90° (*1*), 60° (*2*), 45° (*3*), 30° (*4*), 0 (*5*). Other fitting parameters are: $\gamma_{f\perp,\|}$ = 11 cm^{-1}, $\nu_{p\perp}$ = 90 cm^{-1}, $\gamma_{p\perp}$= 150 cm^{-1}; $\nu_{p\|}$ = 100 cm^{-1}, $\gamma_{P\|}$ = 170 cm^{-1}. Inset demonstrates in details the $R_T(\nu)$ curves within the range 550…630 cm^{-1}.

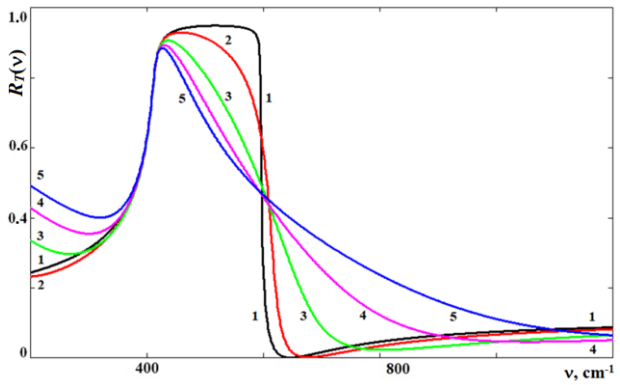

Fig. 4. $R_T(\nu)$ of ZnO single crystal at $E \perp C$, $\gamma_{f\perp}$ = 11 cm^{-1}, $\nu_{p\perp} = \gamma_{p\perp}$ = 1 (*1*), 250 (*2*), 500 (*3*), 750 (*4*), and 1000 cm^{-1} (*5*).

3.2.2. IRR spectra of ZnO ceramic samples

Fig. 5a shows experimental IRR spectra of unpolished (curve *1*) and polished (curve *2*) undoped ZnO ceramic samples as well as simulated $R_T(\nu)$ spectra for polished sample for both *C*-axis orientations – $E \perp C$ (curve *3*) and $E \parallel C$ (curve *4*). Simulation was performed, like to that in the case of ZnO single crystal, by using the Kramers–Kronig analysis [14, 15], equations (1)–(3) and the parameters given in Table 2.

As can be seen from Fig. 5a, after polishing the IRR intensity increases within the spectral range 400…600 cm^{-1} without any spectrum changing in other ranges. Contrary to this, variation of the free carrier concentration affects significantly the IRR intensity in the frequency range 600…1000 cm^{-1}, too. This allows distinguishing the effect of surface roughness from the effect of carrier concentration.

Comparison of the IRR spectra of ZnO single crystals and ZnO ceramics (see Figs 2 and 5) suggests that they are similar. It means that the parameters given in Table 2 along with Eqs (1) to (3) permitted to simulate the IRR spectra of both single crystals and ZnO ceramics with proper accuracy.

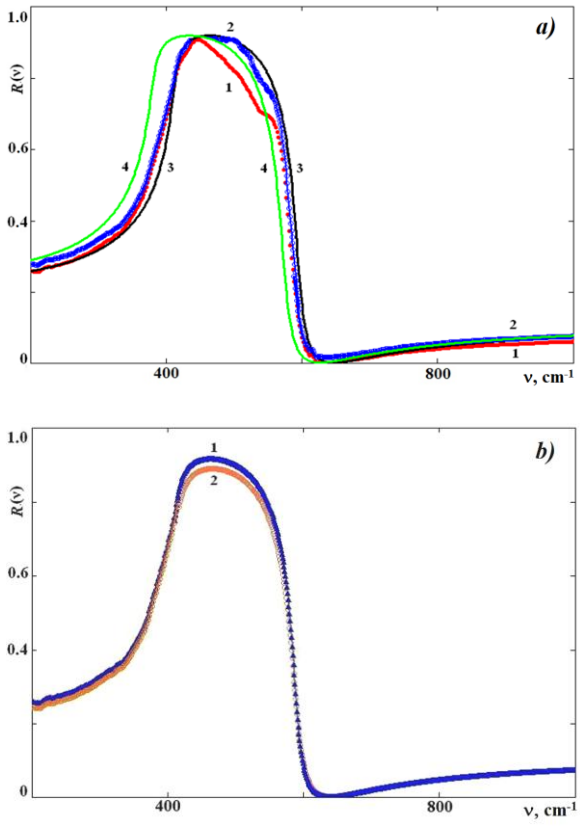

Fig. 5. (a) experimental $R_E(\nu)$ of undoped unpolished (curve *1*) and polished (curve *2*) samples and simulated $R_T(\nu)$ for polished sample: *3* – simulation for $E \perp C$ at ν_P = 450 cm^{-1}, γ_P = 2400 cm^{-1}; γ_f = 13 cm^{-1}; *4* – simulation for $E \parallel C$ at ν_P = 420 cm^{-1}, γ_P = 2200 cm^{-1}; γ_f = 13 cm^{-1} ($\delta = 0.35 \cdot 10^{-2}$), (*b*) – experimental $R_E(\nu)$ spectra of polished undoped (*1*) and Mn-doped (*2*) ceramics, $E \perp C$.

It is worth to point out that XRD data showed random orientation of the ZnO grains in ceramic sample, whereas the shape of corresponding IRR spectrum is close to that simulated for orientation $E \perp C$. The contribution of $E \parallel C$ polarization is negligible. It could manifest only in the range 390…400 cm^{-1} (Fig. 3), where a slight deviation of the $R_E(\nu)$ curve from the $R_T(\nu)$ one for $E \perp C$ is observed. This result can be explained by the fact that the contribution of the polarization $E \perp C$ to the IRR spectrum can be given by all crystallites, whatever their orientation in the regard of direction of light incidence, while for polarization $E \parallel C$ only crystallites with a certain direction of the *C*-axis with respect to the direction of light incidence give the contribution to reflection spectrum. Indeed, as it was mentioned above, only in the case of excitation of A_1 vibration in the *Z*-direction, which coincides with the direction of the *C*-axis, it is possible to observe the IRR spectrum for the case $E \parallel C$. Otherwise, the IRR spectrum for $E \perp C$ orientation will be registered.

Thus, the IRR spectra of ZnO ceramics can be simulated taking into account only the $E \perp C$ orientation. This modeling allows estimating the concentration of free carriers and their mobility in ZnO crystallites. In this case, to prevent the effect of surface roughness, simulation has to be performed in the frequency range above the LO phonon frequency. Indeed, as shown in Table 3, the surface roughness has a little effect on the evaluation of free carrier concentration when this simulation is used. Thus, despite the possible contribution of the surface roughness to the IRR spectrum, the conductivity, concentration and mobility of free carriers can be obtained even for an unpolished sample.

As Fig. 5b shows, the IR reflection spectrum of manganese-doped ZnO ceramics is very close to that of undoped sample. The crystallite parameters obtained by fitting the IRR spectra of undoped sample are close to the parameters evaluated from the IRR spectra of doped ceramics (Table 3).

3.2.3. Direct current conductivity

To get insight on the reliability of the IRR method for studying the ceramics and to demonstrate its importance in the case of doped samples, DC conductivity measurements were performed for the samples described above. For the undoped samples (their IRR spectrum is shown in Fig. 5), the DC conductivity value was $\sigma = 10\ \Omega^{-1} \cdot cm^{-1}$, which is close to the value obtained from the IR reflection spectrum. It indicates reliability of the IR spectroscopy data. At the same time, for Mn-doped ceramics the DC electrical conductivity was several orders of magnitude lower ($\sigma = 7 \cdot 10^{-3}\ \Omega^{-1} \cdot cm^{-1}$). In addition, in this sample, unlike to the undoped one, nonlinear current-voltage characteristic was observed (Fig. 6) contrary to linear current-voltage characteristic detected for undoped ZnO.

Table 3. Parameters of ZnO crystallites in unpolished and polished undoped and polished Mn-doped ceramic samples.

Sample	ν_p, cm^{-1}	γ_p, cm^{-1}	γ_f, cm^{-1}	Concentration n_0, cm^{-3}	Conductivity σ, Ω^{-1} cm^{-1}	Mobility μ, $cm^2/(V \cdot s)$
polished undoped sample	270	2000	13	$8.4 \cdot 10^{17}$	15.03	11.18
unpolished undoped sample	280	2000	15	$9.02 \cdot 10^{17}$	16.17	11.19
polished Mn-doped sample	300	2100	18	$1.0 \cdot 10^{18}$	17.6	1.65

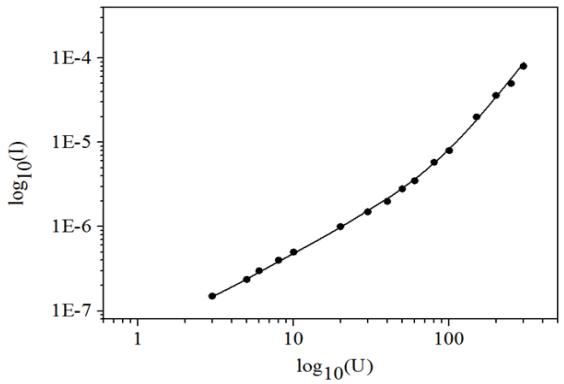

Fig. 6. Current-voltage characteristic of the Mn-doped ZnO ceramic sample.

The difference between the data obtained from IR spectra and DC measurements, which is observed for the doped sample, indicates the presence of low- and high-resistance regions, which is confirmed by the nonlinearity of the current-voltage characteristic. As follows from the modeling of IR reflection spectra, low-resistance regions are ZnO crystallites, while high-resistance ones are associated with barriers at their boundaries or with intergranular spaces, which may include impurity-related phases.

As it is known, doping the ZnO ceramics with Mn is used to produce varistors [8, 26]. Such doping leads to the appearance of Schottky barriers at the grain boundaries due to the adsorption of oxygen on the crystallite surface [27, 28]. The oxygen adsorption becomes possible due to the presence of a Mn-contained interlayer between ZnO grains [22] that can be distinguished by Raman scattering method. This process does not occur in undoped ceramics or ceramics with the uniform impurity distribution, which explains the proximity of the data obtained by IR reflection and DC measurements for undoped sample. The conclusion about the absence of barriers in undoped ceramics is also consistent with the experimental data given in [26].

4. Conclusions

Undoped and manganese-doped ZnO ceramics were studied using X-ray diffraction and external IR reflection methods. The electrophysical parameters obtained by modeling of the reflection spectra were compared with the electrical characteristics obtained by direct current measurements. To determine the effect of the crystallite orientation and the concentration of free carriers on the IR reflection spectra, the modeling of ZnO single crystal spectra and their comparison with experimental ones were performed. Based on the analysis of experimental and theoretical spectra of single crystals and ceramics, it has been shown that the IR reflection spectra of ceramics can be modeled using the parameters found for single crystals.

It has been shown that the predominant contribution to the reflection spectra of ceramics is given by the crystallites with the orientation $E \perp C$, which allows modeling the spectra, with account of only this orientation.

It has been found that the surface roughness affects the IR reflection spectra mainly in the frequency range 450…550 cm^{-1}, while the range above LO phonon frequency, relevant for estimating of the electrophysical parameters of the crystallites, remains unchanged. It has been shown that the electrophysical parameters of unpolished ceramics (obtained by modeling of IR spectra in the range above LO phonon frequency) and polished one coincide, which allows estimation of these parameters regardless of the surface roughness.

Comparison of the electrophysical parameters obtained by modeling of the experimental spectra with the data obtained from DC measurements shows that for undoped ceramics they agree well, which confirms the applicability of the IR spectroscopy method to determine the electrophysical parameters of ceramics. In the case of Mn-doped ceramics, the DC conductivity is much less than that determined by simulation of the reflection spectra. This is explained by the presence of barriers at the boundaries of the crystallites related with oxygen adsorption.

Acknowledgements

This work was supported by the National Research Fund of Ukraine from the state budget, project 2020.02/0380 “Structural transformations and non-equilibrium electronic processes in broadband oxides and their solid solutions”.

References

1. Demianets L.N., Kostomarov D.V., Kuz'mina I.P., Pushko S.V. Mechanism of growth of ZnO single crystals from hydrothermal alkali solutions. *Crystallogr. Rep.* 2002. **47**. P. S86–S98. https://doi.org/10.1134/1.1529962.
2. Zhang X., Herklotz F., Hieckmann E., Weber J., Schmidt P. Vapor phase growth of ZnO single crystals. *J. Vac. Sci. Technol. A.* 2011. **29**. 03A107. https://doi.org/10.1116/1.3553461.
3. Hüpkes J., Müller J., Rech B. Texture Etched ZnO:Al for Silicon Thin Film Solar Cells. *Springer Series in Materials Science.* 2008. P. 359–413. https://doi.org/10.1007/978-3-540-73612-7_8.
4. Wachau A., Schulte J., Agoston P. *et al*. Sputtered Zn(O,S) buffer layers for CIGS solar modules – from lab to pilot production. *Prog. Photovolt.: Res. Appl.* 2017. **25**. P. 696–705. https://doi.org/10.1002/pip.2880.
5. Klingshirn C.F., Waag A., Hoffmann A., Geurts J. Zinc Oxide. From Fundamental Properties towards Novel Applications. *Springer Series in Materials Science.* Springer-Verlag, 2010. https://doi.org/10.1007/978-3-642-10577-7.
6. Reynolds D.C., Look D.C., Jogai B. Optically pumped ultraviolet lasing from ZnO. *Solid State Commun.* 1996. **99**. P. 873–875. https://doi.org/10.1016/0038-1098(96)00340-7.
7. Frieiro J.L., Guillaume C., López-Vidrier J. *et al*. Toward RGB LEDs based on rare earth-doped ZnO. *Nanotechnology.* 2020. **31.** P. 465207. https://doi.org/10.1088/1361-6528/abadc9.
8. Han J., Senos A.M.R., Mantas P.Q. Varistor behaviour in Mn doped ZnO ceramics. *J. Eur. Ceram. Soc.* 2002. **22**. P. 1653–1660. https://doi.org/10.1016/S0955-2219(01)00484.
9. Sendi R. Impact of sintering temperatures on conduction behaviors of ZnO nanoparticles- and MnO-doped SnO_2-based thick film varistors obtained by screen printing. *Modern Phys. Lett. B.* 2019. **33**. P. 1950336. https://doi.org/10.1142/S0217984919503366.
10. Chou C., Chang Y., Lin P., Liu F. Cu-doped ZnO nanowires as highly efficient continuous flow photocatalysts for dynamic degradation of organic pollutants. *J. Photochem. Photobiol. A: Chem.* 2017. **347**. P. 1–8. https://doi.org/10.1016/j.jphotochem.2017.07.010.
11. Baran M.P., Korsunskaya N.E., Stara T.R. *et al.* Graded ZnS/ZnS_xO_{1-x} heterostructures produced by oxidative photolysis of zinc sulfide: Structure, optical properties and photocatalytic evolution of molecular hydrogen. *J. Photochem. Photobiol. A: Chem.* 2016. **329**. P. 213–220. https://doi.org/10.1016/j.jphotochem.2016.07.003.
12. Markevich I.V., Borkovska L.V., Venger Ye.F. *et al*. Electrical, optical and luminescent properties of zinc oxide single crystals. *Ukr. J. Phys. (Reviews).* 2018. **13**. P. 57–76.
13. Korsunska N., Borkovska L., Polischuk Yu. *et al.* Photoluminescence, conductivity and structural study of terbium doped ZnO films grown on different substrates. *Mater. Sci. Semicond. Process.* 2019. **94**. P. 51–56. https://doi.org/10.1016/j.mssp.2019.01.041.
14. Venger E.F., Melnichuk A.V., Melnichuk L.Ju., Pasechnik Ju.A. Anisotropy of the ZnO single crystal reflectivity in the region of residual rays. *phys. status solidi B.* 1995. **188**. P. 823–831. https://doi.org/10.1002/pssb.2221880226.
15. Melnichuk O., Melnichuk L., Venger E. Phonon and plasmon–phonon interactions in ZnO single crystals and thin films, in: *Oxide-Based Materials and Structures: Fundamentals and Applications* (Eds. R. Savkina, L. Khomenkova). 2020. Taylor & Francis Group. CRC Press. https://doi.org//10.1201/9780429286728.
16. Mel'nichuk A.V., Mel'nichuk L.Y., Pasechnik Y.A. Surface plasmon-phonon polaritons of hexagonal zinc oxide. *Tech. Phys.* 1998. **43.** P. 52–55. https://doi.org/10.1134/1.1258935.
17. Venger E.V., Melnichuk L.Yu., Melnichuk O.V., Pasichnyk Yu.A. Influence of the plasmon-phonon coupling on the reflectance coefficient in one-axis polar ZnO semiconductor. *Ukr. J. Phys.* 2000. **45**. P. 976–984.
18. Melnichuk O.V., Melnichuk L.Yu., Korsunska N.O., Khomenkova L. Yu., Venger Ye.F. Optical and electrical properties of Tb–ZnO/SiO_2 structure in the infrared spectral interval. *Ukr. J. Phys.* 2019. **64**. P. 434–441. https://doi.org/10.15407/ujpe64.5.434.
19. Korsunska N., Borkovska L., Khomenkova L. *et al.* Transformations in the photoluminescent, electrical and structural properties of Tb^{3+} and Eu^{3+} co-doped ZnO films under high-temperature. *J. Lumin.* 2020. **217**. P. 116739. https://doi.org/10.1016/j.jlumin.2019.116739.
20. Venger Ye.F., Melnichuk O.V., Melnichuk L.Yu., Semikina T.V. IR spectroscopic study of thin ZnO films grown using the atomic layer deposition method. *Ukr. J. Phys.* 2016. **61**. P. 1059–1066. https://doi.org/10.15407/ujpe61.12.1053.
21. Melnichuk O., Melnichuk L., Venger Ye. *et al.* Investigation of plasmon-phonon interaction in ZnO films deposited on Si substrates in pure argon and argon-oxygen mixed. *Semicond. Sci. Technol.* 2020. **35**. P. 095034. https://doi.org/10.1088/1361-6641/ab9397.
22. Nosenko V., Korsunska N., Vorona I. *et al.* The mechanism of formation of interface barriers in ZnO:Mn ceramics. *SN Appl. Sci.* 2020. **2**. P. 979. https://doi.org/10.1007/s42452-020-2754-8.
23. Spitzer W.G., Kleinman D.A. Infrared lattice bands of quartz. *Phys. Rev.* 1961. **121**. P. 1324–1335. https://doi.org/10.1103/physrev.121.1324-1335.

24. Vinogradov E.A., Dorofeev I.A. Thermally stimulated electromagnetic fields of solids. *Physics-Uspekhi*. 2009. **52**. P. 425–459. https://doi.org/10.3367/UFNr.0179.200905a.0449.
25. Poulet H., Mathieu J.P. *Vibrational Spectra and Symmetry of Crystals*. Gordon and Breach, New York, London, Paris, 1976.
26. Ronard-Haret J.C. Influence of the sintering temperature on the electrical and luminescence properties of Mn-doped ZnO. *Solid State Ionics.* 2004. **167**. P. 355–366. https://doi.org/10.1016/j.ssi.2004.01.019.
27. Boumezoued A., Guergouri K., Zaabat M., Recham D., Barille R. Investigation of structural and electrical properties of manganese doped ZnO varistors prepared from nanopowders. *J. Nanosci. Nanotech. Applications.* 2018. **2**. P. 1–7.
28. Shinde V.R., Gujar T.P., Lokhande C.D., Mane R.S., Han S-H. Mn-doped and undoped ZnO films: A comparative structural, optical and electrical properties study. *Mater. Chem. Phys.* 2006. **96**. P. 326–330. https://doi.org/10.1016/j.matchemphys.2005.07.045.

Authors and CV

Oleksandr Melnichuk, Doctor of Physical and Mathematical Sciences (2001), Professor, Excellence in Education of Ukraine, Vice-Rector for Research and International Relations of Mykola Gogol Nizhyn State University. The area of scientific interest is in the field of surface plasmon-phonon excitations in hexagonal ZnO and 6H-SiC semiconductors and structures on their basis. Author of more than 300 scientific and methodological works in the field of semiconductor and dielectric physics, solid state physics, mathematical modeling, problems of higher and secondary school.
https://orcid.org/0000-0002-6768-8765

Nadiia Korsunska, Doctor of Physical and Mathematical Sciences (1986), Professor (1997), Laureate of the State Prize of the USSR, Leading scientist of the Laboratory of multifunctional composite materials at the V. Lashakryov Institute of Semiconductor Physics. Her scientific interest covers the non-equilibrium recombination processes; electronically stimulated defect reactions, diffusion and defect drift processes in semiconductors and dielectrics, degradation of materials and devices, physics of low-dimensional and nanostructured materials. Author of more than 300 scientific papers, 9 patents in the field of physics of semiconductors and dielectrics.
https://orcid.org/0000-0002-4778-5074

Iryna Markevich, Doctor of Physical and Mathematical Sciences (1997), Leading scientist of the Laboratory of multifunctional composite materials at the V. Lashakryov Institute of Semiconductor Physics. The scope of scientific activity concerns physics of defects and their reactions stimulated by different factors, elaboration of composite materials for photonic and microelectronic applications, diffusion of defects and their drift in electrical field, the processes of degradation of materials and devices. Author of more than 150 papers.
https://orcid.org/0000-0001-8425-5198

Vitaliy Boyko, PhD in Solid State Physics (2012), researcher at the Institute of Physics. His scientific activity concerns optical and opto-electronic properties in mono-, poly- and low-dimensional structures. Scientific activities are related to optical and optoelectronic properties of monocrystalline, polycrystalline and small-sized structures. The subject of research is defects and their influence on the optical properties of solids. Research methods – luminescence, various types of infrared spectroscopy, optoelectrical, including the use of cryogenic temperatures. The author of more than 20 papers.
https://orcid.org/0000-0001-5146-0531

Yuliia Polishchuk, PhD in Solid State Physics (2019), junior researcher at the V. Lashkaryov Institute of Semiconductor Physics. Author over 20 articles. The area of her scientific interests includes solid state physics, X-ray powder diffraction and materials science.
https: //orcid.org/0000-0002-4116-3653

Zinoviia Tsybrii, Doctor of Physical and Mathematical Sciences (2021), Head of the Laboratory of Physics and Technology for Formation of Semiconductor Structures at the V. Lashkaryov Institute of Semiconductor Physics. Her current research interests include physics of semiconductors and their interaction with infrared light, elaboration and fabrication of infrared and terahertz detectors. She is the author of more than 100 papers and patents.
https://orcid.org/0000-0003-1718-5569

Lyudmyla Melnichuk, PhD in Physical and Mathematical Sciences, Associate Professor, Excellence in Education of Ukraine. Main scientific interest covers plasmon-phonon interaction in anisotropic semiconductor materials. Author of more than 120 scientific and scientific-methodical works in the field of semiconductor physics, solid state physics, problems of higher school. https://orcid.org/0000-0001-5524-5732

Yevgen Venger, Doctor of Physical and Mathematical Sciences, Professor, Corresponding Member of the National Academy of Sciences of Ukraine, Head of the Department of Semiconductor Heterostructures at the V. Lashkaryov Institute of Semiconductor Physics. Author of more than 500 publications, 40 patents, 24 textbooks and manuals. He is one of the founders of polariton optoelectronics. His research interests include physics and technology of semiconductor materials, hetero- and hybrid structures and devices (thin-film solar cells, photoresistors, new types of photo-converters, selective short-wavelength sensors, *etc*.), as well as the modeling of different physical processes in semiconductors and dielectrics.
https://orcid.org/0000-0003-1508-1627

Vasyl Kladko, Doctor of Physical and Mathematical Sciences, Corresponding Member of the National Academy of Sciences of Ukraine, Head of the Department of Structural and Elemental Analysis of Materials and Systems at the V. Lashkaryov Institute of Semiconductor Physics. Author of more than 300 publications. His research interests cover solid-state physics, dynamical theory of diffraction of radiation, X-ray optics, X-ray diffraction analysis of semiconductor crystals, hetero- and nanosystems.
https://orcid.org/0000-0002-1531-4219

Larysa Khomenkova, Doctor of Physical and Mathematical Sciences, Senior Researcher at the Laboratory of multifunctional composite materials of V. Lashkaryov Institute of Semiconductor Physics. Author of more than 170 scientific publications in the field of materials science. The main activity concerns elaboration of multifunctional composite materials and the study of their properties for microelectronic and photonic applications.
https://orcid.org/0000-0002-5267-5945

Особливості спектрів дзеркального інфрачервоного відбивання кераміки на основі оксиду цинку

О.В. Мельничук, Н.О. Корсунська, І.В. Маркевич, В.В. Бойко, Ю.О. Поліщук, З.Ф. Цибрій, Л.Ю. Мельничук, Є.Ф. Венгер, В.П. Кладько, Л.Ю. Хоменкова

Анотація. Виготовлено нелеговану та леговану манганом кераміку оксиду цинку та досліджено її структурні, оптичні та електричні властивості. Показано, що метод інфрачервоної спектроскопії може бути застосований для визначення електрофізичних параметрів керамічних зразків. При цьому для моделювання спектрів інфрачервоного відбивання таких зразків можна використовувати параметри, одержані для монокристалів ZnO. Виявлено, що основний внесок у спектри інфрачервоного відбивання керамічних зразків надають зерна ZnO з орієнтацією осі *C*, перпендикулярної до напрямку вектора електричного поля ($\vec{E} \perp C$). Установлено, що шорсткість поверхні проявляється в цих спектрах переважно в діапазоні 450…550 см$^{-1}$, що дає незначний ефект у діапазоні частот вищих за частоту LO-фонона. Проведено оцінку електрофізичних параметрів нелегованих та легованих манганом зразків. Установлено, що у разі нелегованої кераміки отримані результати збігаються з результатами прямих вимірювань електропровідності зразків. Для керамічних зразків, легованих манганом, пряме вимірювання їх провідності дає значення, яке значно менше за величину, одержану при моделюванні спектрів інфрачервоного відбивання. Така відмінність пояснюється утворенням бар'єрів на границях зерен ZnO, легованих манганом.

Ключові слова: ZnO, кераміка, інфрачервона спектроскопія, легування, провідність.